Engineering ER-stress dependent non-conventional mRNA splicing

Weihan Li[1, *], Voytek Okreglak[1, 3], Jirka Peschek[1], Philipp Kimmig[1, 4], Meghan Zubradt[2], Jonathan Weissman[2], Peter Walter[1, *]

[1] Department of Biochemistry and Biophysics and Howard Hughes Medical Institute, University of California San Francisco, CA 94143, USA

[2] Department of Cellular and Molecular Pharmacology and Howard Hughes Medical Institute, University of California San Francisco, CA 94143, USA

[3] Current address: Calico Life Sciences LLC, South San Francisco, CA 94080, USA

[4]Current address: Institute of Biochemistry, ETH Zürich, Zürich, Switzerland

***: Corresponding authors**

Abstract

The endoplasmic reticulum (ER) protein folding capacity is balanced with the protein folding burden to prevent accumulation of un- or misfolded proteins. The ER membrane-resident kinase/RNase Ire1 maintains ER protein homeostasis through two fundamentally distinct processes. First, Ire1 can initiate a transcriptional response through a non-conventional mRNA splicing reaction to increase the ER folding capacity. Second, Ire1 can decrease the ER folding burden through selective mRNA decay. In *Saccharomyces cerevisiae* and *Schizosaccharomyces pombe,* the two Ire1 functions have been evolutionarily separated. Here, we show that the respective Ire1 orthologs have become specialized for their functional outputs by divergence of their RNase specificities. In addition, RNA structural features separate the splicing substrates from the decay substrates. Using these insights, we engineered an *S. pombe* Ire1 cleavage substrate into a splicing substrate, which confers *S. pombe* with both Ire1 functional outputs.

Introduction

In eukaryotes, the vast majority of secretory and transmembrane proteins are folded in the endoplasmic reticulum (ER). The ER protein folding homeostasis is maintained by a collective of signaling pathways, termed the unfolded protein response (UPR) (Walter and Ron, 2011, Ron and Walter, 2007). The most evolutionarily conserved branch of the UPR is mediated by the ER-transmembrane kinase/endoribonuclease (RNase) Ire1. Direct binding of unfolded proteins to Ire1's ER lumenal domain triggers Ire1 to oligomerize and form foci (Gardner and Walter, 2011, Karagoz et al., 2017, Credle et al., 2005, Aragon, van Anken et al., 2009). In turn, Ire1 oligomerization activates Ire1's cytosolic kinase/RNase domain (Korennykh et al., 2009), which restores ER homeostasis through two functional outputs. First, Ire1 initiates a process of non-conventional cytosolic splicing of *XBP1* mRNA (in metazoans) or *HAC1* mRNA (in *S. cerevisiae*). Translation of the spliced mRNA produces a transcription factor Xbp1 (Hac1 in *S. cerevisiae*), which drives a large transcriptional program to adjust the ER's protein-folding capacity according to the protein folding load in the ER lumen (Cox et al., 1993, Mori et al., 1993, Yoshida et al., 2001, Calfon et al., 2002, Sidrauski et al., 1996). Second, Ire1 can reduce the ER folding burden by cleaving a set of mRNAs encoding ER-target proteins. The initial Ire1-mediated cleavage leads to mRNA degradation, in a process termed regulated Ire1-dependent decay (RIDD) (Hollien and Weissman, 2006, Hollien et al., 2009, Kimmig, Diaz et al., 2012). The mechanism that

distinguishes the non-conventional mRNA splicing from RIDD has largely remained unknown.

Interestingly, the two Ire1 modalities co-exist in metazoan cells (Hollien and Weissman, 2006, Hollien et al., 2009, Moore and Hollien, 2015), yet are evolutionarily separated in the two yeast species, *S. cerevisiae* and *S. pombe*. The UPR in *S. cerevisiae* engages Ire1 exclusively in mRNA splicing, whereas in *S. pombe* it engages Ire1 exclusively in RIDD. There is no detectable RIDD in *S. cerevisiae* and no *HAC1*/ *XBP1* ortholog in *S. pombe*, nor is there a corresponding transcriptional program (Niwa et al., 2005, Kimmig, Diaz et al., 2012). It is intriguing to note that the fundamental task of maintaining ER protein homeostasis can be achieved by two radically different processes catalyzed by two distantly related Ire1 orthologs. The two yeast species, *S. cerevisiae* and *S. pombe,* therefore provide a unique opportunity to dissect the two Ire1 functional outputs, which has remained an unsolved challenge in metazoans. Here, we set out to exploit this opportunity.

Results

S. pombe and *S. cerevisiae* Ire1's cytosolic domains are functionally divergent

Despite their common role as UPR effectors and conserved domain structure (Fig. 1A), *S. pombe* and *S. cerevisiae* Ire1 orthologs share 29% sequence identity, and sequence variation may confer Ire1's functional divergence. To explore this notion, we swapped the homologous *IRE1* genes between the two yeast species by expressing *S. cerevisiae* Ire1 in *Δire1 S. pombe* cells and, *vice versa*, *S. pombe* Ire1 in *Δire1 S. cerevisiae* cells. To this end, we constructed strains in which we integrated the foreign *IRE1* genes into the genomes of the other yeast such that their expression was regulated by the host species-endogenous *IRE1* promoters and the resulting mRNAs contained host species-endogenous 5' and 3' untranslated regions (UTR). The *IRE1* genes contained sequences encoding FLAG-tags that we inserted into an unstructured loop in their ER-lumenal domains in a position known to preserve Ire1 function (Rubio et al., 2011). In both yeasts, the foreign genes expressed Ire1 at comparable levels (Fig. 1B & C, lanes 3). However, when grown on plates containing tunicamycin, a drug that blocks N-linked glycosylation and induces ER stress, the foreign Ire1s failed to support cell growth of either *S. pombe* and *S. cerevisiae* cells (Fig. 1D & E, lanes 3), indicating that *S. pombe* and *S. cerevisiae* Ire1s are not interchangeable.

There are two plausible, not mutually exclusive scenarios that could explain the failure of cross-species complementation: i) the foreign Ire1 lumenal domains fail to sense ER stress, or ii) the foreign Ire1 cytosolic domains fail to recognize species-appropriate RNA substrates. Since the Ire1 lumenal domains have lower sequence identity (21%) than the cytosolic kinase/RNase domains (45%), we first swapped the Ire1 lumenal domains, generating chimeras with foreign lumenal domains and host species-endogenous transmembrane/cytosolic domains. Both chimeras supported growth on tunicamycin plates, suggesting that the divergent Ire1 lumenal domains share a conserved mechanism to sense ER stress and transduce the signal across ER membrane (Fig. 1D & E, lanes 4). Next, we swapped the Ire1 transmembrane/cytosolic domains. These Ire1 chimeras failed to restore growth on tunicamycin plates of both *S. pombe* and *S. cerevisiae* cells (Fig. 1D & E, lanes 5), indicating that the Ire1 transmembrane/cytosolic domains cause the Ire1 functional incompatibility when expressed in the opposing yeast. As a control, we expressed FLAG-tagged host species-endogenous Ire1s into *Δire1* strains of both yeasts. These strains phenocopied the wild type (WT) cells on tunicamycin plates (Fig. 1D & E, lanes 6). We again confirmed by immunoblotting that all of the FLAG-tagged Ire1 constructs were stably expressed at near-endogenous level in both yeasts (Fig. 1B & C).

We next asked whether the Ire1 constructs would process the host species-appropriate RNA substrates in *S. pombe* and *S. cerevisiae* cells. To this end, we performed Northern blot and qPCR analyses to measure cleavage and subsequent

down-regulation of *GAS2* mRNA, which is a RIDD target in *S. pombe* cells (Kimmig, Diaz et al., 2012). We performed the Northern blot in *Δski2 S. pombe*, in which the RNA 3' to 5' decay machinery is impaired so that the *GAS2* mRNA 5' cleavage fragments can be detected in the gel. Of the different Ire1 variants, only the Ire1 chimera bearing the *S. pombe* cytosolic domain cleaved the *GAS2* mRNA (Fig. 1—figure supplement 1A) and decreased the mRNA level (Fig. 1F), consistent with the growth phenotype. In *S. pombe*, Ire1 also cleaves the *BIP1* mRNA within its 3'UTR, producing a truncated mRNA with an increased half-life (Kimmig, Diaz et al., 2012). To assess *BIP1* mRNA processing, we performed qPCR analysis using two pairs of primers, one pair bracketing the Ire1 cleavage site and the other pair bracketing a region upstream of it (Fig. 1G, schematic insert, *black* vs. *grey* arrows), reporting on uncleaved only and both *BIP1* mRNA species (i.e. total *BIP1* mRNA), respectively. As expected, upon tunicamycin-induced ER stress in WT cells uncleaved *BIP1* mRNA levels decreased while total *BIP1* mRNA level increased (Fig. 1G, lanes 1, 2). As shown in Figure 1G, Ire1 variants bearing the *S. pombe* cytosolic domain processed *BIP1* mRNA, whereas Ire1 variants bearing the *S. cerevisiae* cytosolic domain did not. This result is further validated by Northern blot analysis of *BIP1* mRNA (Fig. 1—figure supplement 1B).

Correspondingly in *S. cerevisiae* cells, we examined *HAC1* mRNA splicing by PCR across its splice junction. Consistent with the cell growth phenotype on tunicamycin, the two Ire1 constructs bearing the *S. pombe* cytosolic domains did not splice *HAC1* mRNA in *S. cerevisiae* cells (Fig. 1H, lanes 6, 10). By contrast, the Ire1

chimera bearing the *S. pombe* lumenal domain and *S. cerevisiae* cytosolic domains spliced *HAC1* mRNA (Fig. 1H, lane 8), albeit at reduced efficiency compared to WT *S. cerevisiae* Ire1 (Fig. 1H, lane 2). We confirmed the activity of the various Ire1 constructs in *HAC1* mRNA splicing by monitoring UPR dynamics with a *HAC1* mRNA-derived splicing reporter (Fig. 1—figure supplement 2A & B) previously described (Aragon, van Anken et al., 2009, Zuleta et al., 2014). The reduced *HAC1* mRNA splicing efficiency observed for Ire1 bearing the *S. pombe* lumenal domain (Fig. 1H, lane 8, and Fig. 1—figure supplement 2B, column 4) can be explained by the observation that the *S. pombe* lumenal domain mediates a lower degree of oligomerization than its *S. cerevisiae* counterpart, as demonstrated by the reduced ability of Ire1-mCherry fusion constructs to form foci visible by fluorescent microscopy (Fig. 1—figure supplement 2C). Consistent with previous studies (Aragon, van Anken et al., 2009), the insertion of the mCherry module into the Ire1 cytosolic linker, which connects Ire1 transmembrane domain and cytosolic kinase/RNase domain, did not affect its ability to sustain cell growth (Fig. 1—figure supplement 2D).

Ire1 kinase/RNase domains have distinct RNase specificity

To further confine the Ire1 region giving rise of the species differences in outputs, we expressed an Ire1 chimera that, in addition to the *S. cerevisiae* lumenal domain, also included the *S. cerevisiae* transmembrane and cytosolic linker domains fused to the *S. pombe* kinase/RNase domain. This chimeric Ire1 weakly rescued cell

160 growth and mildly restored the *HAC1* mRNA splicing upon ER stress (Fig. 2A lane 4,
161 & Fig. 2B lane 6), compared to the chimera containing *S. pombe* transmembrane and
162 cytosolic linker domains, although both constructs were expressed at similar
163 protein levels (Fig. 2C). This result indicates that the major difference lies in the
164 kinase/RNase domains, but that the transmembrane and cytosolic linker domains
165 can afford a marginal rescue, most likely by reintroducing cytosolic linker elements
166 that facilitate *HAC1* mRNA docking (van Anken et al., 2014).
167
168 To study the differences by which the Ire1 kinase/RNase domains select
169 their respective substrate mRNAs, we purified recombinant *S. cerevisiae* and *S.*
170 *pombe* kinase/RNase domains and performed *in vitro* RNA cleavage assays. The *S.*
171 *cerevisiae* Ire1 kinase/RNase efficiently cleaved a cognate 29-nucleotide RNA
172 hairpin derived from the 3' splice site of *S. cerevisiae HAC1* mRNA (Fig. 2D). By
173 contrast, under the same conditions the *S. pombe* Ire1 kinase/RNase cleaved the *S.*
174 *cerevisiae HAC1* mRNA-derived substrate ~60-fold slower (Fig. 2D). Reciprocally,
175 the *S. pombe* Ire1 kinase/RNase efficiently cleaved a cognate 32-nucleotide RNA
176 hairpin derived from the cleavage site in *S. pombe BIP1* mRNA and cognate RNA
177 hairpins derived from the RIDD cleavage sites in *S. pombe SPAC4G9.15* and *PLB1*,
178 whereas *S. cerevisiae* Ire1 kinase/RNase cleaved the *BIP1* mRNA-derived substrate
179 and the *S. pombe SPAC4G9.15* >500-fold slower and *PLB1* mRNA-derived hairpins
180 ~100-fold slower (Fig. 2E, F, G). These *in vitro* data validate and expand the
181 conclusions from the experiments conducted *in vivo*, suggesting that the different

Ire1 RNase specificities separate their functional outputs and that they are not dependent on other cellular factors such as associated proteins or lipids.

Ire1 kinase/RNase domains recognize distinct RNA sequence and structural features

Ire1 recognizes its substrates based on both RNA sequence and structural features. The required RNA sequence motifs were characterized previously and differ between species: for *S. cerevisiae* Ire1 a nucleotide sequence of CNG|CNGN or CNG|ANGN ("|" indicates the Ire1 cleavage position) situated in a strictly conserved 7-membered loop is required (Gonzalez et al., 1999). By contrast, for *S. pombe* Ire1 a three-nucleotide sequence of UG|C is required and no additional structural features have yet been characterized (Kimmig, Diaz et al., 2012, Guydosh et al., 2017). To fill this gap in our knowledge, we examined the RNA secondary structures *in vivo*. To this end, we treated the *S. pombe* cells with dimethyl sulfate (DMS), which allows detection of exposed (unpaired and not blocked by proteins) adenine/cytosine residues (illustrated as green dots in Fig. 3A). RNA was extracted, reverse transcribed and deep-sequenced. The DMS modifications stop reverse transcriptase and generate truncated DNA fragments that we mapped through deep sequencing. We then used identified unpaired bases to guide *in silico* RNA secondary structure predictions (Rouskin et al., 2014). For example, near one of the *GAS2* mRNA cleavage sites, five bases, labeled in green in Figure 3B, have high DMS modification signals. In the RNA folding software mfold (Zuker, 2003), we provided the

205 constraint such that these five residues are unpaired and obtained the predicted
206 RNA secondary structure (Fig. 3C). In this structure, the *GAS2* mRNA forms a 9-
207 membered stem loop with the cleavage consensus sequence UG|C located near the
208 center of the loop. In similar analyses of 13 additional *S. pombe* Ire1 substrate mRNA
209 cleavage sites previously identified by both Kimmig, Diaz et al. and Guydosh et al.
210 (Guydosh et al., 2017, Kimmig, Diaz et al., 2012), we found in all of them cleavage
211 sites located near the center of loops in RNA stem-loop structures (Fig. 3—figure
212 supplement 1 A, B). By contrast to those found in *S. cerevisiae HAC1* mRNA, the
213 predicted loops were of variable sizes, with the smallest being a 3-membered loop
214 (e.g., the *SPAC4G9.15* mRNA cleavage site) and the largest being a 9-membered loop
215 (e.g., the *BIP1* mRNA cleavage site). We summarize that *S. pombe* Ire1 is tolerant to
216 loop size variation, while the *S. cerevisiae* Ire1 stringently recognizes 7-membered
217 stem loops. Thus, the *S. cerevisiae* and *S. pombe* Ire1 recognize distinct RNA
218 sequence and structural features (Fig. 3D).
219
220 A prediction of this model is that RNAs that combine *S. cerevisiae* and *S.*
221 *pombe* Ire1 motifs should be substrates to Ire1 from either species. To test this
222 prediction, we analyzed a substrate satisfying criteria for both species. Specifically,
223 we examined a substrate predicted to form a 7-membered stem loop with the
224 sequence CUG|CAGC, meeting the criteria of both the *S. cerevisiae* Ire1 motif
225 (CNG|CNGN) and the *S. pombe* Ire1 motif (UG|C). Indeed, both enzymes cleaved this
226 RNA *in vitro* with similar efficiency, in strong support of our model (Fig. 3E).
227

We further challenged the model *in vivo* by modifying the *S. pombe BIP1* mRNA. First, we replaced the Ire1 cleavage site in the 3' UTR of *BIP1* mRNA with a sequence derived from the *S. cerevisiae HAC1* mRNA 5' splice site. This modification is predicted to change the endogenous 9-membered loop to a 7-membered one. The new construct ('*BIP1-HAC1* hybrid mRNA') contained the sequence AG|C, which is different from the *S. pombe* Ire1 sequence motif UG|C. In support of our model, *S. pombe* Ire1 failed to cleave the *BIP1-HAC1* hybrid mRNA upon UPR induction (Fig. 3G, bar 3 & 4, Fig. 3—figure supplement 2A, B). Next, we mutated the non-cognate A to a cognate U, such that the *S. pombe* Ire1 cleavage motif UG|C was restored. Indeed, the single nucleotide change restored the *S. pombe* Ire1 cleavage (Fig. 3G, bar 5 & 6, Fig. 3—figure supplement 2C). Taken together, we conclude that the Ire1 orthologs in *S. cerevisiae* and *S. pombe* have divergent substrate preferences.

Engineering non-conventional mRNA splicing in *S. pombe*

While these results revealed the differences between the *S. cerevisiae* and *S. pombe* UPR at the step of Ire1 cleavage, it was not clear what determines the fates of the RNA cleavage fragments, i.e. RNA ligation in *S. cerevisiae* and RNA degradation in *S. pombe*. To address this question, we tested whether *S. pombe* cells contain functional mRNA ligation machinery. To this end, we expressed the *S. cerevisiae HAC1* mRNA-derived splicing reporter (Fig. 1—figure supplement 2A) in *Δire1 S. pombe* cells, bearing genomic copies of various Ire1 constructs. A chimeric Ire1 bearing the *S. pombe* cytosolic domain failed to splice the reporter mRNA, in

agreement with our model (Fig. 4A, lane 5 & 6). Interestingly, both Ire1 constructs bearing the *S. cerevisiae* cytosolic domains successfully spliced the reporter mRNA (Fig. 4A, lanes 1-4). Thus, the *S. pombe* cells ligated the mRNA cleavage fragments as long as the correct RNA substrates were provided. This result suggested that features in the RNA substrates determine their fate post Ire1 cleavage.

Recently, we reported that in mammalian cells the *XBP1* mRNA actively participates in the splicing reaction. In particular, a conformational RNA rearrangement promotes *XBP1* mRNA intron ejection and exon ligation (Peschek, Acosta-Alvear et al., 2015). We wondered if this mechanism could be the factor that diverges the fates of the RNA cleavage fragments. To address this question, we aimed to synthetically create the Ire1-dependent non-conventional mRNA splicing reaction in *S. pombe* cells initiated by endogenous *S. pombe* Ire1. First, we identified the analogous RNA conformational rearrangement in *S. cerevisiae HAC1* mRNA. To obtain a *HAC1*-derived RNA splicing cassette optimized for *S. pombe* Ire1, we then engineered the two Ire1-cleavage sites at the splice junctions to match the *S. pombe* Ire1 UG|C motif and pruned the intron (originally 252 bp in *S. cerevisiae*) to the very residues predicted to be critical for the mRNA conformational rearrangement (30 bp). Finally, we inserted the *S. pombe*-optimized mRNA splicing cassette into *S. pombe BIP1* mRNA, replacing its endogenous Ire1 cleavage site (Fig. 4B, Fig. 4–figure supplement 1). Indeed, we found that the *BIP1* mRNA containing the synthetic splicing cassette was spliced in *S. pombe* upon induction of ER stress (Fig. 4C lane 2). Sequencing of the lower band in Figure 4C (lane 2) verified the designed identity of

the splicing product (Fig. 4D). To show that insertion of the splicing cassette triggers mRNA splicing independent of particular flanking elements, we inserted the splicing cassette into the 3'UTR of another synthetic mRNA. In this case, we constructed a synthetic mRNA containing the 5' UTR of tubulin (*NDA2*) mRNA, the open reading frame of a *GAS2* mutant mRNA in which all of its RIDD cleavage sites were mutated, and the 3' UTR of *NDA2* mRNA with the inserted splicing cassette (Fig. 4E). As for the mRNA described above, this construct was efficiently spliced in *S. pombe* upon ER stress (Fig. 4F). Thus, we conclude that the substrate RNA structure determines the fate of the RNA cleavage fragments.

Discussion

"What I cannot create, I do not understand" (Richard Feynman). Inspired by this quote, we engineered *S. pombe* cells to carry out a non-conventional mRNA splicing reaction that does not occur in this species naturally. This feat was enabled by a combination of a detailed mechanistic characterization of the differences in Ire1-dependent mRNA processing between two yeast species reported in this paper and by functional insights gleaned previously from a characterization of the mammalian *XBP1* mRNA splicing mechanism (Peschek, Acosta-Alvear et al., 2015). Two main conclusions emerged from this study. First, the evolutionary divergence of Ire1's substrate specificity determines the set of mRNAs that are cleaved in either species. Second, features in the mRNAs determine the distinct fates of the severed mRNA fragments. *S. pombe* can be coopted to carry out the core non-conventional mRNA splicing reaction with fidelity, as long as it is provided with a spliceable RNA substrate that matches the specificity requirements of its endogenous Ire1. Albeit not optimized in evolution for efficiency of the reaction, no other components (such as the RNA ligase) need to be fundamentally specialized to mediate the core splicing reaction.

Ire1 orthologs in *S. cerevisiae* and *S. pombe* recognize their cognate mRNA substrates by discriminating both sequence and structural features. *S. pombe* Ire1 RNase specificity is more promiscuous, and has a broad substrate scope, in line with its role to initiate degradation of many ER-bound mRNAs to reduce the ER's protein

folding burden. By contrast, *S. cerevisiae* Ire1's RNase specificity is very stringent and specialized with *HAC1* mRNA being as its only substrate in the cell (Niwa et al., 2005), in line with its role to produce a single transcription activator to drive UPR target genes. In mammals, two paralogs of Ire1 are expressed in a tissue-specific manner (Tsuru et al., 2013, Bertolotti et al., 2001). Ire1α, which performs both *XBP1* mRNA splicing and RIDD, recognizes a similar but longer RNA sequence motif, CUG|CAG, displayed in stem-loop structures (Maurel et al., 2014). Interestingly, the loop sizes that Ire1α recognizes differ between the *XBP1* mRNA cleavage sites and RIDD cleavage sites, with the two cleavage sites on *XBP1* mRNA to be conserved 7-mer loops (Hooks and Griffiths-Jones, 2011), while the cleavage sites on RIDD substrates vary in range from 9-mers to 5-mers (Fig. 4—figure supplement 2). This suggests that mammalian Ire1α may display two distinct modes of RNase activity—a more stringent mode of RNase activity observed on 7-mer stem-loop RNAs (*XBP1* mRNA and *BLOC1S* mRNA) and a more promiscuous mode of RNase activity on RNA substrates with variable loop sizes. As shown here, these two modes have been cleanly separated in evolution between *S. cerevisiae* and *S. pombe* Ire1. Hence it seems plausible that mammalian Ire1α may switch selectively into one or the other state, perhaps in response to the timing of UPR activation or certain physiological conditions, which could be reflected in particular oligomeric states, post-translational modifications, or other effectors yet to be discovered.

Ire1α is more efficient in *XBP1* mRNA splicing, while Ire1β prefers to cleave ribosomal RNA (Iwawaki et al., 2001, Nakamura et al., 2011, Imagawa et al., 2008).

Pairwise sequence alignment did not reveal an obvious similarity signatures that would distinguish the Ire1 species performing for RIDD, i.e., *S. pombe* Ire1 and Ire1β, from those engaged in mRNA splicing, i.e., *S. cerevisiae* Ire1 and Ire1α (Fig. 4—figure supplement 3A, B). On the substrate side, two Ire1β cleavage sites both located on rRNA, have been mapped to date. They share a common sequence of G|C at the cleavage site. Previous studies indicated that differences in Ire1α's and Ire1β's RNase domains lead to their functional distinction (Imagawa et al., 2008). We did not observed cleavage of rRNA by *S. pombe* Ire1 (Fig. 1—figure supplement 1A, B); mammalian Ire1β's activity to do so may therefore reflect a specialization that is not generalizable to all Ire1 RNases that perform RIDD. Therefore, modulating Ire1's RNase specificity to regulate its mode of action emerges as a general theme for different species, as well as for different tissues within the same species.

In *S. cerevisiae* cells, apart from the *HAC1* mRNA, other mRNAs contain the *S. cerevisiae* Ire1 cleavage motif, yet are not cleaved (Niwa et al., 2005). This is explained by spatial coordination. *HAC1* mRNA is targeted to Ire1 upon stress, utilizing a specific signal in the *HAC1* mRNA 3'UTR (Aragon, van Anken et al., 2009), conferring exquisite specificity that renders *HAC1* mRNA the sole substrate of the reaction. Although two other Ire1 substrate RNAs have been reported (Tam et al., 2014), we have not been able to reproduce this result. By contrast to the dedicated mRNA targeting in *S. cerevisiae*, *S. pombe* and mammalian cells target *XBP1* mRNA and most RIDD substrates to the ER via the signal recognition particle (SRP) pathway (Hollien and Weissman, 2006, Hollien et al., 2009, Yanagitani et al., 2009,

354 Yanagitani et al., 2011, Plumb et al., 2015). In this way, *S. pombe* and mammalian
355 Ire1 efficiently sample through substrate RNAs at ER periphery, which they cleave
356 more promiscuously. We presume that in our experimental set-up, the chimeric
357 *BIP1*-mRNA containing the splicing cassette would highjack the SRP-mediated
358 targeting route initiated by the BiP1 signal sequence, as we previously showed for
359 other RIDD substrate mRNAs (Kimmig, Diaz et al., 2012).
360
361 After Ire1 cleavage, RNA fragments are ligated or degraded, depending on the
362 substrate RNA structures. According to this notion, in mammalian cells where
363 splicing and RIDD co-exist, we predict that *XBP1* mRNA splicing and RIDD substrate
364 degradation are separated post Ire1 cleavage. The two cleavage sites on the *XBP1*
365 mRNA are coordinated by a zipper-like RNA structure, which enable the exons to be
366 held in juxtaposition and ligated by the cytosolic tRNA ligase (Peschek, Acosta-
367 Alvear et al., 2015, Sidrauski et al., 1996, Jurkin et al., 2014, Lu et al., 2014,
368 Kosmaczewski et al., 2014). By contrast, cleavage sites on the RIDD substrates lack
369 such coordination and the cleavage fragments are further degraded.
370
371 Our study revealed that Ire1's RNase specificity and its RNA substrate
372 structure separate Ire1's modes of action, opening the door to identify residues that
373 shape Ire1's RNase specificity. In this way, it should now become possible to design
374 metazoan Ire1s that favor mRNA splicing over RIDD, and *vice versa*, enabling us to
375 discriminate the biological significance of the two Ire1 functional outputs separately
376 in physiological and pathological contexts.

Acknowledgement

The *Δire1 S. pombe* strain was a generous gift from the Krogan lab (UCSF). We thank Ignacio Zuleta, Benjamin Heineike and Alain Bonny for their help and discussion on automated flow cytometry. We thank Wallace Marshall, Marc Shuman and members of the Walter lab for their insightful discussions. This work was supported by UCSF-Zaffaroni Fellowship (WL), the Human Frontier Science Program (JP, PK), National Science Foundation grant 1144247 (MZ), the Genentech Foundation (MZ) and CRSB (Center for RNA Systems Biology; grant P50 GM102706 to JSW). PW and JSW are Investigators of the Howard Hughes Medical Institute.

Competing Financial Interests

The authors declare no competing financial interests.

Figure 1

***S. pombe* and *S. cerevisiae* Ire1 have functionally conserved stress sensing ER-lumenal domains and divergent cytosolic domains.** (A) Cartoon illustration of lumenal domain (LD), transmembrane/cytosolic linker domain (TMD+L) and kinase/RNase domain (KR) for *S. pombe* (*Sp*) (*blue*) and *S. cerevisiae* (*Sc*) Ire1 (*orange*). (B, C) Expression levels of *S. cerevisiae* Ire1 (128 kD), *S. cerevisiae* lumenal *S. pombe* cytosolic Ire1 (126 kD), *S. pombe* lumenal *S. cerevisiae* cytosolic Ire1 (125 kD) and *S. pombe* Ire1 (122 kD) in *S. pombe* (B) and *S. cerevisiae* cells (C). Extracts were immunoblotted for 3xFLAG-Ire1. Ponceau stain (B) or Pgk1 (C) was used as loading control. (D, E) Cell growth assay on tunicamycin (Tm) plates. Serial dilutions of *S. pombe* (D) or *S. cerevisiae* (E) cells, which expressed the indicated Ire1 constructs, were spotted onto plates containing 0.05 μg/ml (B) or 0.1 μg/ml (C) of Tm. Plates were photographed after incubation at 30° C for 4 days. (F, G) qPCR assay for *S. pombe GAS2* (F) or *BIP1* (G) mRNA fold change upon 1 μg/ml Tm treatment for 1 h. Experiments were done in triplicates. In (G), uncleaved (*dark grey*) or total (*light grey*) *BIP1* mRNA was detected using the corresponding PCR primers illustrated as arrows in the schematic insert. The red dashed line indicates the Ire1 cleavage position on *BIP1* mRNA. (H) Detection of *S. cerevisiae HAC1* mRNA splicing by RT-PCR across the splice junction. Cells were treated with or without 1 μg/ml of Tm for 1 h.

Figure 1—figure supplement 1

Ire1 chimeras with *S. pombe* cytosolic domain cleave *BIP1* and *GAS2* mRNA in *S. pombe*. Northern blots of *S. pombe GAS2* (A) and *BIP1* (B) mRNA. Cells were treated with 1 μg/ml of Tm for 1 h.

Figure 1—figure supplement 2

Ire1 oligomeric state determines the *HAC1* mRNA splicing dynamics in *S. cerevisiae* cells. (A) Illustration of the *HAC1* mRNA derived splicing reporter. The splicing reporter contains a part of the *HAC1* mRNA 5' exon replaced by the green fluorescent protein (GFP) coding sequence. In the unspliced reporter mRNA, translation is inhibited by a translation block formed by the intron and 5'UTR (indicated by the red arrow). Upon splicing, intron is removed and translation begins. (B) Measuring the *HAC1* mRNA splicing dynamics in *S. cerevisiae* using automated flow cytometry. After 1.5 h of incubation, either no Tm or 0.25 μg/ml, 0.5 μg/ml, 1 μg/ml, 2 μg/ml of Tm was added. Then, we monitored the splicing dynamics for 10 h. The splicing dynamics under various conditions is plotted. *Green* lines represent the strains of interest, which expressed indicated Ire1 variants, and the *black* line represents WT control strain under the same condition. (C) Examining Ire1 foci formation in *S. cerevisiae* cells via fluorescence microscopy with or without 1 μg/ml Tm treatment for 20 min. (D) Growth assay on Tm plate for *S. cerevisiae* cells expressing Ire1 constructs with or without mCherry inserted into the cytosolic linker. The inserted mCherry does not affect Ire1's ability to alleviate ER stress.

Figure 2

***S. pombe* and *S. cerevisiae* Ire1 have distinct RNase specificity.** (A) Growth assay for *S. cerevisiae* cells expressing indicated Ire1 constructs on Tm plates, as Figure 1E. (B) Measuring *HAC1* mRNA splicing, as Figure 1H. (C) Comparing the expression levels of the indicated 3xFLAG-tagged Ire1 chimeras using immunoblotting. Ponceau stain was used as loading control. (D, E, F, G) *In vitro* RNA cleavage assays. 5'-radiolabeled hairpin RNA substrates were incubated with 12.5 μM *S. cerevisiae* or *S. pombe* Ire1 kinase/RNase domains (KR) at 30° C for the indicated time. (D) Hairpin RNA substrate derived from the 3' splice site of *S. cerevisiae HAC1* mRNA. The calculated k_{obs} is 9.4 ± 0.9 × 10^{-4} s^{-1} for *S. cerevisiae* Ire1 KR and 0.15 ± 0.01 × 10^{-4} s^{-1} for *S. pombe* Ire1 KR. (E) Hairpin RNA substrate derived from the Ire1 cleavage site on *S. pombe BIP1* mRNA. The calculated k_{obs} is 0.079 ± 0.0006 × 10^{-4} s^{-1} for *S. cerevisiae* Ire1 KR and 37.3 ± 4.4 × 10^{-4} s^{-1} for *S. pombe* Ire1 KR. (F) Hairpin RNA substrate derived from the Ire1 cleavage site on *S. pombe SPAC4G9.15* mRNA, encoding a gene of unknown function. The calculated k_{obs} was below our detection limit for *S. cerevisiae* Ire1 KR and 15.6 ± 2.2 × 10^{-4} s^{-1} for *S. pombe* Ire1 KR. (G) Hairpin RNA substrate derived from the Ire1 cleavage site on *S. pombe PLB1* mRNA. The calculated k_{obs} is 0.2 ± 0.003 × 10^{-4} s^{-1} for *S. cerevisiae* Ire1 KR and 19.0 ± 2.5 × 10^{-4} s^{-1} for *S. pombe* Ire1 KR.

Figure 3

***S. pombe* and *S. cerevisiae* Ire1 recognize distinct RNA sequence and structural features.** (A) Illustration of RNA structural mapping by DMS modifications. Dimethyl sulfate (DMS) allows detection of unpaired adenine and cytosine RNA bases (*green* dots). (B) The normalized DMS modification signals near the Ire1 cleavage site on *S. pombe GAS2* mRNA (cleavage site is indicated by the *red* dashed line). The positions with high DMS modification signals are labeled in *green* and the previously identified *S. pombe* Ire1 UG|C motif is labeled in *red*. (C) *In sillico* RNA secondary structure prediction of the Ire1 cleavage site on *GAS2* mRNA. Structure prediction was constrained by forcing the positions with high DMS modification signals (*green*) to be unpaired. (D) RNA sequence and structural motifs recognized by the *S. cerevisiae* and *S. pombe* Ire1. (E) *In vitro* cleavage assay using an RNA hairpin derived from human *XBP1* mRNA 3' splice site, which is predicted to be a shared substrate for *S. cerevisiae* and *S. pombe* Ire1 KR. The calculated k_{obs} is 16.7 ± 2.3 × 10^{-4} s^{-1} for *S. cerevisiae* Ire1 KR and 38.9 ± 4.0 × 10^{-4} s^{-1} for *S. pombe* Ire1 KR. (F) Illustrations of the *S. pombe BIP1* mRNA variants and (G) their uncleaved (*dark grey*) or total (*light grey*) mRNA fold change upon ER stress in *S. pombe* cells. Experiments were done in triplicates.

Figure 3—figure supplement 1

***S. pombe* Ire1 cleaves at UG|C positioned near the center of loops in RNA stem-loop structures.** (A) A list of all 14 *S. pombe* Ire1 mRNA cleavage sites, which were independently identified by both Kimmig, Diaz et al. and Guydosh et al. (Guydosh et al., 2017, Kimmig, Diaz et al., 2012). The UG|C motifs are labeled in *red*. The positions with high DMS modification signals are labeled in *green*. (B) Predicted RNA secondary structures of *S. pombe* Ire1 cleavage sites. DMS modification signals were used to guide the secondary structure prediction of *S. pombe* Ire1 mRNA cleavage sites. The *red* dashed lines indicate the Ire1 cleavage sites.

Figure 3—figure supplement 2

Ire1 cleavage sites on *BIP1* mRNA variants. Sequence and predicted RNA secondary structures of Ire1 cleavage sites on (A) *S. pombe BIP1* mRNA, (B) *BIP1-HAC1* hybrid mRNA and (C) *BIP1-HAC1* hybrid mRNA with an A to U mutation. The part included in the dashed box is derived from *S. cerevisiae HAC1* mRNA 5' splice site.

Figure 4

Engineering the Ire1-mediated non-conventional mRNA splicing in *S. pombe* cells. (A) Measuring the non-conventional mRNA splicing in *S. pombe* cells, which were transformed with the *S. cerevisiae HAC1* mRNA splicing reporter and the indicated Ire1 constructs. Cells were treated with 1 μg/ml Tm for 1 h. (B) Illustration of the engineered *S. pombe BIP1* mRNA splicing variant. (C) Measuring the nonconventional mRNA splicing of the engineered *S. pombe BIP1* mRNA splicing variant. Experimental conditions are the same as those for Figure 4A. (D) Sequencing reads of the spliced *BIP1* mRNA. The schematic illustrations (E) and the splicing assays (F) of the synthetic splicing substrates in *S. pombe*. Cells were treated with 1 μg/ml Tm for 1 h.

Figure 4—figure supplement 1

The splicing cassette in the engineered *S. pombe BIP1* mRNA splicing variant.

The part included in the dashed box is the inserted synthetic splicing cassette. The *red* dashed lines indicate the Ire1 cleavage sites. The *S. pombe* Ire1 UG|C motifs are labeled in red.

Figure 4—figure supplement 2

The Ire1 α cleavage sites on *XBP1* mRNA and a RIDD targets. Red dashed lines mark the cleavage sites and the red letters indicate the previously identified sequence motif.

Figure 4—figure supplement 3

The sequence alignment of the kinase/RNase domains of Ire1 α , Ire1β, the *S. cerevisiae* Ire1 and the *S. pombe* Ire1. (A) The sequence alignment and colored with BoxShade Server. (B) The sequence identities between the indicated pairs of Ire1 constructs.

Materials and Methods:

Strains, plasmids and growth conditions

Standard *S. cerevisiae* and *S. pombe* genome editing and growth conditions were used (Moreno et al., 1991, Guthrie and Fink, 2002). Strains used in this study are listed in the Table 1. Specifically, all Ire1 constructs have a 3x FLAG-tag in their lumenal domains replacing an unstructured region (255-274 in *S. pombe* and 267-286 in *S. pombe*). *S. cerevisiae* Ire1 domain boundaries were previously described (Rubio et al., 2011), *S. pombe* Ire1 domains were determined by sequence alignment with *S. cerevisiae* Ire1. Specifically, the lumenal domain is 1-526 for *S. cerevisiae* and 1-507 for *S. pombe*. The transmembrane/cytosolic linker is 527-672 for *S. cerevisiae* and 508-651 for *S. pombe*. Kinase/RNase is 673-1115 for *S. cerevisiae* and 652-1073 for *S. pombe*. Ire1 constructs were integrated into the *HO* locus in *S. cerevisiae* (backbone plasmid: HO-Poly-KanMX4-HO) and *Leu* locus in *S. pombe* (backbone plasmid: pJK148). *S. pombe BIP1* variants were integrated at the *BIP1* locus through homologous recombination and uracil selection. The mCherry-tagged Ire1 constructs and the splicing reporter were previously described (Aragon, van Anken et al., 2009).

Growth assay

Serial dilutions of *S. cerevisiae* or *S. pombe* cells were spotted onto YPD plates with 0.1 μg/ml tunicamycin (for *S. cerevisiae*) or YE5S plates with 0.05 μg/ml

544 tunicamycin (for *S. pombe*). Plates were photographed after incubating at 30° C for 4
545 days.
546
547 **Immunoblotting**
548 For both *S. cerevisiae* and *S. pombe* cells, total protein was isolated from yeast
549 cultures growing at exponential phase by vortexing with glass beads in 8 M urea, 50
550 mM Hepes, pH 7.4, and 1% sodium dodecylsulfate (SDS). Samples were boiled and
551 then centrifuged at 16,000 x g for 10 min. A sample containing 20 μg total protein
552 was separated using electrophoresis and then transferred to nitrocellulose. The
553 3xFLAG-tagged Ire1 was probed with monoclonal anti-FLAG antibody (Sigma
554 F3165).
555
556 **qPCR assays**
557 Total RNA was purified from yeast cultures using phenol extraction (Kohrer and
558 Domdey, 1991). RNA samples were resuspended in RNase-free water and quantified
559 by spectrophotometry. cDNA was synthesized by reverse transcription using
560 random hexamer DNA primers (Thermo Fisher Scientific), SuperScript II Reverse
561 Transcriptase (Thermo Fisher Scientific) and 1 μg total RNA as described previously
562 (Kimmig, Diaz et al., 2012). 1% of the cDNAs was employed for qPCR reactions using
563 SYBR green qPCR kit (Bio-Rad). qPCR was performed in triplicates using CFX96
564 Touch Real-Time PCR Detection System (Bio-rad). qPCR primers are listed in Table
565 2. mRNA levels were normalized to *NDA2* mRNA in *S. pombe*.
566

567 ***In vivo* mRNA splicing assay**

568 cDNA was synthesized the same way as described in the qPCR section. Then we
569 used Phusion High-Fidelity PCR Kit (NEB) and performed PCR with cDNA and a set
570 of primers across the splice junction. For *HAC1* mRNA, the forward primer was
571 ATGGAAATGACTGATTTTGAACTAACTAGTAATTCG. The reverse primer was
572 TCATGAAGTGATGAAGAAATCATTCAATTCAAATG. The PCR was performed for 26
573 cycles with annealing temperature of 51.5° C and extension time of 30 s. For the *S.*
574 *pombe BIP1* mRNA containing the splicing cassette, the forward primer was
575 GAATCGTGACTCTATAGCCATTAACA. The reverse primer was
576 CAATTATTGTCAGTTCCACAAAGC. The PCR was performed for 36 cycles with
577 annealing temperature of 63.4° C and extension time of 15 s. For *S. cerevisiae HAC1*
578 mRNA derived splicing reporter expressed in *S. pombe* cells, the forward primer was
579 GAACTACAAGACACGTGCTGAAG. The reverse primer was
580 GATGAAGAAATCATTCAATTCAAATG. The PCR was performed for 60 cycles with
581 annealing temperature of 63.2° C and extension time of 20 s. For the synthetic
582 splicing substrate in *S. pombe*, the forward primer was
583 CTCATTTAGATTAGCAATTCAAATG. The reverse primer was
584 GATTAGATCAACAATTCAAATGATC. The PCR was performed for 40 cycles with
585 annealing temperature of 59.7° C and extension time of 20 s.
586

587 **Recombinant protein purification**

588 *S. cerevisiae* Ire1 kinase/RNase was purified as previously described (Korennykh et
589 al., 2009). Details of the *S. pombe* Ire1 kinase/RNase purification will be described in

590 a separate paper. Briefly, *S. pombe* Ire1 kinase/RNase was N-terminally fused with
591 Glutathione S-transferase (GST) tag through a linker containing Human Rhinovirus
592 (HRV) 3C protease cleavage site, and was regulated by T7 promoter. This *S. pombe*
593 Ire1 kinase/RNase expression cassette was transformed into *E. coli* cells. 16 h after
594 transformation, we mixed and collected all the colonies on the transformation plates
595 by scraping them off from the agar plate into 50 ml of LB medium. After 3-hour
596 incubation at 37° C, the sample was diluted to 12 l of LB medium and further
597 incubated at 37° C until optical density reached 1. Protein expression was induced
598 by adding 0.5 mM IPTG. Then, the culture was incubated at 25° C for 4 h before we
599 pelleted the cells by centrifugation. Cells were resuspended in GST binding buffer
600 (50 mM Tris/HCl pH 7.5, 500 mM NaCl, 2 mM $Mg(OAc)_2$,, 2 mM DTT, 10% Glycerol)
601 and homogenized using high-pressure homogenizer (EmulsiFlex, Avestin). The cell
602 lysate was applied to GST-affinity column and eluted with GST elusion buffer (50
603 mM Tris/HCl pH 7.5, 200 mM NaCl, 2 mM $Mg(OAc)_2$, 2 mM DTT, 10% Glycerol, 10
604 mM glutathione). The column elution was treated with GST-tagged HRV 3C protease
605 (PreScission Protease, GE Health). At the same time, the sample was dialyzed to
606 remove glutathione in the elution buffer. Next, the sample was further purified
607 through negative chromatography by passing through a GST-affinity column (to
608 remove free GST and residue GST-fused Ire1 kinase/RNase) and an anion exchange
609 column (to remove contaminating nucleic acids). Finally, the sample was subject to
610 gel filtration, concentrated to about 14 μM in storage buffer (50 mM Tris/HCl pH
611 7.5, 200 mM NaCl, 2 mM $Mg(OAc)_2$, 2 mM TCEP, 10% Glycerol), and flash frozen in

liquid nitrogen. The final purity, as well as purity at intermediate steps, was assessed by SDS-PAGE using Coomassie blue staining.

In vitro RNA cleavage assays

Short RNA oligos were purchased from Dharmacon, Inc. RNA oligos were gel extracted, acetone precipitated and resuspended in RNase-free water. Then, oligos were 5' end radio-labeled with γ-[^{32}P]-ATP (Perkin Elmer) using T4 polynucleotide kinase (NEB) and cleaned using ssDNA/RNA Clean and Concentrator kit (Zymo Research D7010). To fold the RNA oligos, we heated the RNA oligos to 90° C for 3 min and slowly cooled them down at a rate of 1° C per minute until the temperature reached 10° C. In the Ire1 cleavage assays, the reaction samples contained 12.5 μM of *S. cerevisiae* or *S. pombe* Ire1 kinase/RNase. The cleavage reaction was performed at 30° C in reaction buffer (50 mM Tris/HCl pH 7.5, 200 mM NaCl, 2 mM $Mg(OAc)_2$, 2 mM TCEP, 10% Glycerol). At each time point, an aliquot of 0.75 μl was transferred to 5 μl STOP buffer (10 M urea, 0.1% SDS, 1 mM EDTA, 0.05% xylene cyanol, 0.05% bromophenol blue). RNAs were separated using denaturing 15% urea-PAGE gels (run at 100 V for 90 min). Gels were imaged with a Phosphorimager (Typhoon FLA 9500, GE Health) and the band intensities were quantified using imageJ. The cleaved portion was calculated as the cleaved band intensity divided by the sum of the cleaved band and uncleaved band intensities. The k_{obs} were obtained by fitting the data to first-order ("one-phase") decay equation using Prism. For the cleavage reactions that less than 10% of the substrates were cleaved, because the substrate concentration was approximately constant, the cleavage dynamics was fitted to a

linear equation to obtain k_{obs}. The sequence of hairpin RNA substrate derived from Ire1 cleavage site on *S. pombe BIP1* mRNA is CGCGAGAUAACUGGUGCUUUGUUAUCUCGCG.

The sequence of hairpin RNA substrate derived from Ire1 cleavage site on *S. pombe SPAC4G9.15* mRNA is CCACCACCGAGUAUGCUACUCGGUGGUGG.

The sequence of hairpin RNA substrate derived from *S. cerevisiae HAC1* mRNA 3' splice site is GCGCGGACUGUCCGAAGCGCAGUCCGCGC

The sequence of hairpin RNA substrate derived from *XBP1* mRNA 3' splice site is UGCACCUCUGCAGCAGGUGCA.

Automated flow cytometry

Measuring *S. cerevisiae* UPR dynamics using automated flow cytometry was previously described in detail (Zuleta et al.). Briefly, we co-cultured two *S. cerevisiae* strains, a strain of interest and a control strain. The control strain contained a constitutively expressed mCherry reporter. The signal from the control strain was computationally separate based on its high mCherry level. In an 11.5-hour time course at 30° C, a data point was taken every 20 min. 1.5 h after inoculation, DMSO (as control) or 0.25 μg/ml, 0.5 μg/ml, 1 μg/ml, 2 μg/ml of Tm were added. Splicing dynamics were monitored for another 10 h. The GFP signal was normalized to the signal at time zero.

Probing *in vivo* mRNA structure in *S. pombe* cells

A culture of 15 ml *S. pombe* cells, which were exponentially growing at 30° C, was treated with 400 µl of DMS for 3.5 min. DMS was then quenched by adding 30 ml of solution containing 30% β-mercaptoethanol and 25% isoamyl alcohol. Then, cells were pelleted by centrifugation at 4° C, and washed with 15 ml 30% β-mercaptoethanol. Total RNA was extracted using phenol extraction. Poly(A)+ mRNAs were isolated using poly(A)+ Dynabeads (Invitrogen). The sequencing library was generated and sequenced, and the DMS modifications were computed as previously described (Rouskin et al.).

mRNA secondary structure prediction

Near the Ire1 cleavage sites, we first identified the most highly reactive base and set its DMS modification signal as 1. Then, the DMS modification signal raw data for other bases was normalized proportionally. Finally, we put a 38-base-pair RNA sequence (19 base pair upstream and downstream from the Ire1 cleavage site) into the RNA secondary structure prediction program mfold (Zuker, 2003). Bases with normalized DMS modification signals >0.2 were forced to be single stranded to constrain the RNA folding prediction.

Reference

ARAGON, T., VAN ANKEN, E., PINCUS, D., SERAFIMOVA, I. M., KORENNYKH, A. V., RUBIO, C. A. & WALTER, P. 2009. Messenger RNA targeting to endoplasmic reticulum stress signalling sites. *Nature,* 457**,** 736-40.

BERTOLOTTI, A., WANG, X., NOVOA, I., JUNGREIS, R., SCHLESSINGER, K., CHO, J. H., WEST, A. B. & RON, D. 2001. Increased sensitivity to dextran sodium sulfate colitis in IRE1beta-deficient mice. *J Clin Invest,* 107**,** 585-93.

CALFON, M., ZENG, H., URANO, F., TILL, J. H., HUBBARD, S. R., HARDING, H. P., CLARK, S. G. & RON, D. 2002. IRE1 couples endoplasmic reticulum load to secretory capacity by processing the XBP-1 mRNA. *Nature,* 415**,** 92-6.

COX, J. S., SHAMU, C. E. & WALTER, P. 1993. Transcriptional induction of genes encoding endoplasmic reticulum resident proteins requires a transmembrane protein kinase. *Cell,* 73**,** 1197-206.

CREDLE, J. J., FINER-MOORE, J. S., PAPA, F. R., STROUD, R. M. & WALTER, P. 2005. On the mechanism of sensing unfolded protein in the endoplasmic reticulum. *Proc Natl Acad Sci U S A,* 102**,** 18773-84.

GARDNER, B. M. & WALTER, P. 2011. Unfolded proteins are Ire1-activating ligands that directly induce the unfolded protein response. *Science,* 333**,** 1891-4.

GONZALEZ, T. N., SIDRAUSKI, C., DORFLER, S. & WALTER, P. 1999. Mechanism of non-spliceosomal mRNA splicing in the unfolded protein response pathway. *EMBO J,* 18**,** 3119-32.

GUTHRIE, C. & FINK, G. R. 2002. *Guide to yeast genetics and molecular and cell biology,* Amsterdam ; Boston ; London, Academic Press.

GUYDOSH, N. R., KIMMIG, P., WALTER, P. & GREEN, R. 2017. Regulated Ire1-dependent mRNA decay requires no-go mRNA degradation to maintain endoplasmic reticulum homeostasis in S. pombe. *Elife,* 6, e29216

HOLLIEN, J., LIN, J. H., LI, H., STEVENS, N., WALTER, P. & WEISSMAN, J. S. 2009. Regulated Ire1-dependent decay of messenger RNAs in mammalian cells. *J Cell Biol,* 186**,** 323-31.

HOLLIEN, J. & WEISSMAN, J. S. 2006. Decay of endoplasmic reticulum-localized mRNAs during the unfolded protein response. *Science,* 313**,** 104-7.

719 HOOKS, K. B. & GRIFFITHS-JONES, S. 2011. Conserved RNA structures in the non-
720 canonical Hac1/Xbp1 intron. *RNA Biol,* 8**,** 552-6.
721
722 IMAGAWA, Y., HOSODA, A., SASAKA, S., TSURU, A. & KOHNO, K. 2008. RNase
723 domains determine the functional difference between IRE1alpha and
724 IRE1beta. *FEBS Lett,* 582**,** 656-60.
725
726 IWAWAKI, T., HOSODA, A., OKUDA, T., KAMIGORI, Y., NOMURA-FURUWATARI, C.,
727 KIMATA, Y., TSURU, A. & KOHNO, K. 2001. Translational control by the ER
728 transmembrane kinase/ribonuclease IRE1 under ER stress. *Nat Cell Biol,* 3**,**
729 158-64.
730
731 JURKIN, J., HENKEL, T., NIELSEN, A. F., MINNICH, M., POPOW, J., KAUFMANN, T.,
732 HEINDL, K., HOFFMANN, T., BUSSLINGER, M. & MARTINEZ, J. 2014. The
733 mammalian tRNA ligase complex mediates splicing of XBP1 mRNA and
734 controls antibody secretion in plasma cells. *EMBO J,* 33**,** 2922-36.
735
736 KARAGOZ, G. E., ACOSTA-ALVEAR, D., NGUYEN, H. T., LEE, C. P., CHU, F. & WALTER,
737 P. 2017. An unfolded protein-induced conformational switch activates
738 mammalian IRE1. *Elife,* 6, e30700
739
740 KIMMIG, P., DIAZ, M., ZHENG, J., WILLIAMS, C. C., LANG, A., ARAGON, T., LI, H. &
741 WALTER, P. 2012. The unfolded protein response in fission yeast modulates
742 stability of select mRNAs to maintain protein homeostasis. *Elife,* 1**,** e00048.
743
744 KOHRER, K. & DOMDEY, H. 1991. Preparation of high molecular weight RNA.
745 *Methods Enzymol,* 194**,** 398-405.
746
747 KORENNYKH, A. V., EGEA, P. F., KOROSTELEV, A. A., FINER-MOORE, J., ZHANG, C.,
748 SHOKAT, K. M., STROUD, R. M. & WALTER, P. 2009. The unfolded protein
749 response signals through high-order assembly of Ire1. *Nature,* 457**,** 687-93.
750
751 KOSMACZEWSKI, S. G., EDWARDS, T. J., HAN, S. M., ECKWAHL, M. J., MEYER, B. I.,
752 PEACH, S., HESSELBERTH, J. R., WOLIN, S. L. & HAMMARLUND, M. 2014. The
753 RtcB RNA ligase is an essential component of the metazoan unfolded protein
754 response. *EMBO Rep,* 15**,** 1278-85.
755
756 LU, Y., LIANG, F. X. & WANG, X. 2014. A synthetic biology approach identifies the
757 mammalian UPR RNA ligase RtcB. *Mol Cell,* 55**,** 758-70.
758
759 MAUREL, M., CHEVET, E., TAVERNIER, J. & GERLO, S. 2014. Getting RIDD of RNA:
760 IRE1 in cell fate regulation. *Trends Biochem Sci,* 39**,** 245-54.
761
762 MOORE, K. & HOLLIEN, J. 2015. Ire1-mediated decay in mammalian cells relies on
763 mRNA sequence, structure, and translational status. *Mol Biol Cell,* 26**,** 2873-
764 84.

MORENO, S., KLAR, A. & NURSE, P. 1991. Molecular genetic analysis of fission yeast Schizosaccharomyces pombe. *Methods Enzymol,* 194**,** 795-823.

MORI, K., MA, W., GETHING, M. J. & SAMBROOK, J. 1993. A transmembrane protein with a cdc2+/CDC28-related kinase activity is required for signaling from the ER to the nucleus. *Cell,* 74**,** 743-56.

NAKAMURA, D., TSURU, A., IKEGAMI, K., IMAGAWA, Y., FUJIMOTO, N. & KOHNO, K. 2011. Mammalian ER stress sensor IRE1beta specifically down-regulates the synthesis of secretory pathway proteins. *FEBS Lett,* 585**,** 133-8.

NIWA, M., PATIL, C. K., DERISI, J. & WALTER, P. 2005. Genome-scale approaches for discovering novel nonconventional splicing substrates of the Ire1 nuclease. *Genome Biol,* 6**,** R3.

PESCHEK, J., ACOSTA-ALVEAR, D., MENDEZ, A. S. & WALTER, P. 2015. A conformational RNA zipper promotes intron ejection during non-conventional XBP1 mRNA splicing. *EMBO Rep,* 16**,** 1688-98.

PLUMB, R., ZHANG, Z. R., APPATHURAI, S. & MARIAPPAN, M. 2015. A functional link between the co-translational protein translocation pathway and the UPR. *Elife,* 4, e07426.

RON, D. & WALTER, P. 2007. Signal integration in the endoplasmic reticulum unfolded protein response. *Nat Rev Mol Cell Biol,* 8**,** 519-29.

ROUSKIN, S., ZUBRADT, M., WASHIETL, S., KELLIS, M. & WEISSMAN, J. S. 2014. Genome-wide probing of RNA structure reveals active unfolding of mRNA structures in vivo. *Nature,* 505**,** 701-5.

RUBIO, C., PINCUS, D., KORENNYKH, A., SCHUCK, S., EL-SAMAD, H. & WALTER, P. 2011. Homeostatic adaptation to endoplasmic reticulum stress depends on Ire1 kinase activity. *J Cell Biol,* 193**,** 171-84.

SIDRAUSKI, C., COX, J. S. & WALTER, P. 1996. tRNA ligase is required for regulated mRNA splicing in the unfolded protein response. *Cell,* 87**,** 405-13.

TAM, A. B., KOONG, A. C. & NIWA, M. 2014. Ire1 has distinct catalytic mechanisms for XBP1/HAC1 splicing and RIDD. *Cell Rep,* 9**,** 850-8.

TSURU, A., FUJIMOTO, N., TAKAHASHI, S., SAITO, M., NAKAMURA, D., IWANO, M., IWAWAKI, T., KADOKURA, H., RON, D. & KOHNO, K. 2013. Negative feedback by IRE1beta optimizes mucin production in goblet cells. *Proc Natl Acad Sci U S A,* 110**,** 2864-9.

VAN ANKEN, E., PINCUS, D., COYLE, S., ARAGON, T., OSMAN, C., LARI, F., GOMEZ PUERTA, S., KORENNYKH, A. V. & WALTER, P. 2014. Specificity in endoplasmic reticulum-stress signaling in yeast entails a step-wise engagement of HAC1 mRNA to clusters of the stress sensor Ire1. *Elife,* 3**,** e05031.

WALTER, P. & RON, D. 2011. The unfolded protein response: from stress pathway to homeostatic regulation. *Science,* 334**,** 1081-6.

YANAGITANI, K., IMAGAWA, Y., IWAWAKI, T., HOSODA, A., SAITO, M., KIMATA, Y. & KOHNO, K. 2009. Cotranslational targeting of XBP1 protein to the membrane promotes cytoplasmic splicing of its own mRNA. *Mol Cell,* 34**,** 191-200.

YANAGITANI, K., KIMATA, Y., KADOKURA, H. & KOHNO, K. 2011. Translational pausing ensures membrane targeting and cytoplasmic splicing of XBP1u mRNA. *Science,* 331**,** 586-9.

YOSHIDA, H., MATSUI, T., YAMAMOTO, A., OKADA, T. & MORI, K. 2001. XBP1 mRNA is induced by ATF6 and spliced by IRE1 in response to ER stress to produce a highly active transcription factor. *Cell,* 107**,** 881-91.

ZUKER, M. 2003. Mfold web server for nucleic acid folding and hybridization prediction. *Nucleic Acids Res,* 31**,** 3406-15.

ZULETA, I. A., ARANDA-DIAZ, A., LI, H. & EL-SAMAD, H. 2014. Dynamic characterization of growth and gene expression using high-throughput automated flow cytometry. *Nat Methods,* 11**,** 443-8.

Table 1:

Yeast strains used in this study. All strains are derived from WL001 and WL002. All Ire1 constructs listed below are 3x FLAG-tagged within their lumenal domains.

strain	species	description
yWL001	*Sc*	WT, mat A, *leu2-3,112 TRP1 can1-100 ura3-1 ADE2 his3-11,15*
yWL002	*Sc*	*ire1Δ::NAT^R*
yWL003	*Sc*	*ire1Δ::NAT^R, HO::Sp IRE1*
yWL004	*Sc*	*ire1Δ::NAT^R, HO::Sp*Lum*Sc*Cyto *IRE1*
yWL005	*Sc*	*ire1Δ::NAT^R, HO::Sc*Lum*Sp*Cyto *IRE1*
yWL006	*Sc*	*ire1Δ::NAT^R, HO::Sc IRE1*
yWL007	*Sc*	*ire1Δ::NAT^R, HO::Sc*Lum/transmembrane/linker*Sp*KR *IRE1*
yWL008	*Sc*	WT, *leu2*::*5'hac1-gfp-3'hac1*
yWL009	*Sc*	*ire1Δ::NAT^R, leu2*::*5'hac1-gfp-3'hac1*
yWL010	*Sc*	*ire1Δ::NAT^R, leu2*::*5'hac1-gfp-3'hac1, HO::Sp IRE1*
yWL011	*Sc*	*ire1Δ::NAT^R, leu2*::*5'hac1-gfp-3'hac1, HO:: Sp*Lum*Sc*Cyto *IRE1*
yWL012	*Sc*	*ire1Δ::NAT^R, leu2*::*5'hac1-gfp-3'hac1, HO:: Sc*Lum*Sp*Cyto *IRE1*
yWL013	*Sc*	*ire1Δ::NAT^R, leu2*::*5'hac1-gfp-3'hac1, HO::Sc IRE1*
yWL014	*Sc*	*leu2*::*5'hac1-gfp-3'hac1, his3*::*pTdh3-mCherry*
yWL015	*Sp*	WT, mat h$^+$, *ade6-M210, ura4-D18, leu1-32*
yWL016	*Sp*	*ire1Δ::KAN^R*
yWL017	*Sp*	*ire1Δ::KAN^R, leu1::Sp IRE1*
yWL018	*Sp*	*ire1Δ::KAN^R, leu1::Sp*Lum*Sc*Cyto *IRE1*
yWL019	*Sp*	*ire1Δ::KAN^R, leu1::Sc*Lum*Sp*Cyto *IRE1*
yWL020	*Sp*	*ire1Δ::KAN^R, leu1::Sc IRE1*
yWL021	*Sp*	*ire1Δ::KAN^R, leu1::Sp*Lum*Sc*Cyto *IRE1, ura4::5'hac1-gfp-3'hac1*
yWL022	*Sp*	*ire1Δ::KAN^R, leu1::Sc*Lum*Sp*Cyto *IRE1, ura4::5'hac1-gfp-3'hac1*
yWL023	*Sp*	*ire1Δ::KAN^R, leu1::Sc IRE1, ura4::5'hac1-gfp-3'hac1*
yWL024	*Sp*	*bip1::bip1-hac1* hybrid
yWL025	*Sp*	*bip1::bip1-hac1* hybrid A->U
yWL026	*Sp*	*bip1::bip1* splicing variant
yWL027	*Sp*	*ura4::synthetic* splicing substrate

Table 1:

qPCR primers used in this study.

qPCR primers description	sequence
uncleaved *Sp BiP1* mRNA forward primer	GAATCGTGACTCTATAGCCATTAACA
uncleaved *Sp BiP1* mRNA reverse primer	CAATTATTGTCAGTTCCACAAAGC
total *Sp BiP1* mRNA forward primer	TGGTAAGGTTGATCCCGAAG
total *Sp BiP1* mRNA reverse primer	CATCGAGTTTTTGACGCTGA
Sp GAS2 mRNA forward primer	GTTGTCAACAATGCCTCGAA
Sp GAS2 mRNA reverse primer	CGGTCTCAGAGTTGGTGTCA
Sp NDA2 mRNA forward primer	TCCATGAATCCAACAGCGTA
Sp NDA2 mRNA reverse primer	CTAGTAACGGCAGCCTGGAC

Fig 1 Li et al.

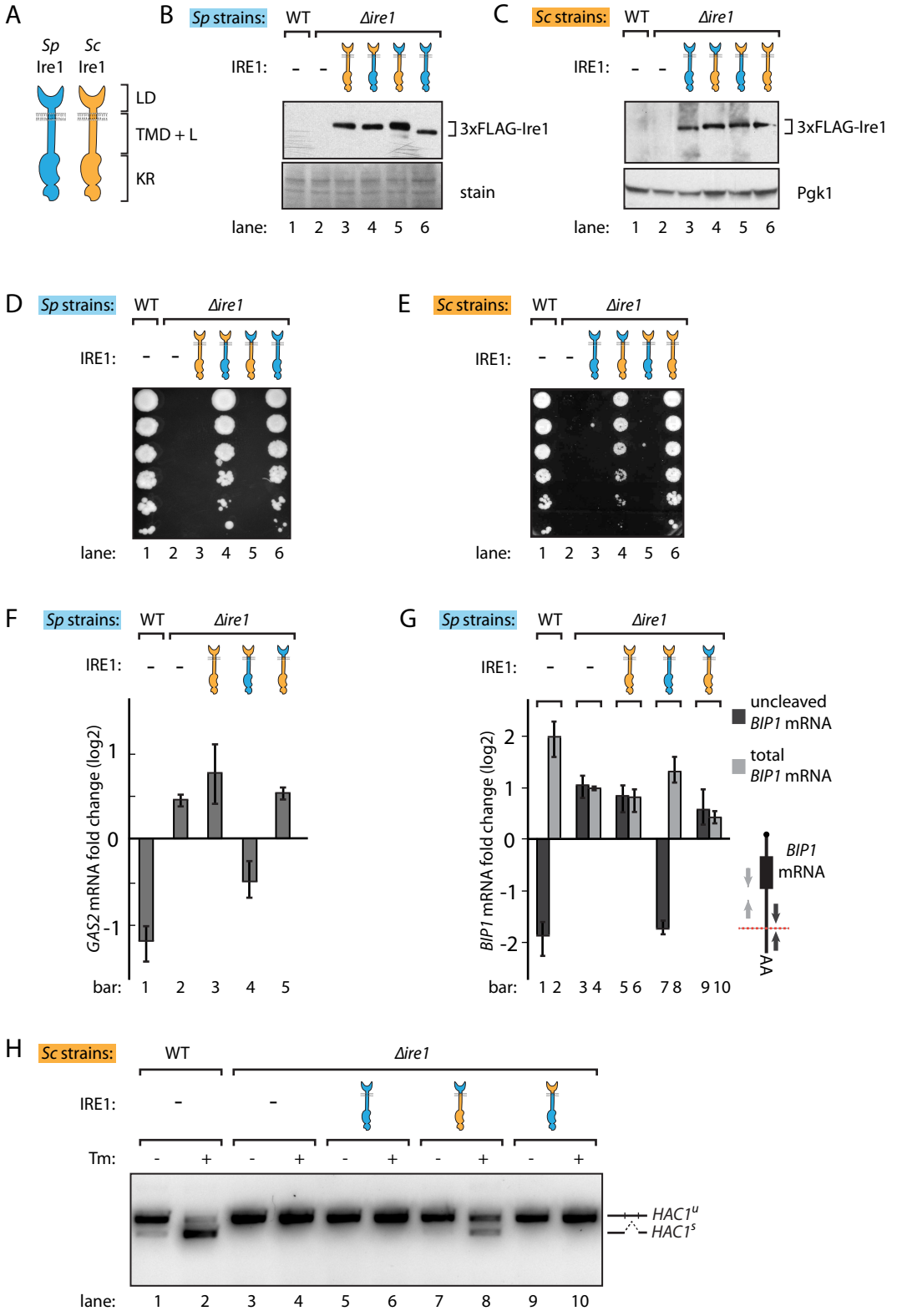
A
Sp Ire1
Sc Ire1
LD
TMD + L
KR
B
Sp strains:
WT
Δire1
IRE1:
3xFLAG-Ire1
stain
lane: 1 2 3 4 5 6
C
Sc strains:
WT
Δire1
IRE1:
3xFLAG-Ire1
Pgk1
lane: 1 2 3 4 5 6
D
Sp strains:
WT
Δire1
IRE1:
lane: 1 2 3 4 5 6
E
Sc strains:
WT
Δire1
IRE1:
lane: 1 2 3 4 5 6
F
Sp strains:
WT
Δire1
IRE1:
GAS2 mRNA fold change (log2)
bar: 1 2 3 4 5
G
Sp strains:
WT
Δire1
IRE1:
BIP1 mRNA fold change (log2)
uncleaved BIP1 mRNA
total BIP1 mRNA
BIP1 mRNA
AA
bar: 1 2 3 4 5 6 7 8 9 10
H
Sc strains:
WT
Δire1
IRE1:
Tm:
HAC1u
HAC1s
lane: 1 2 3 4 5 6 7 8 9 10

Fig. 1-figure supplement 1 Li et al.

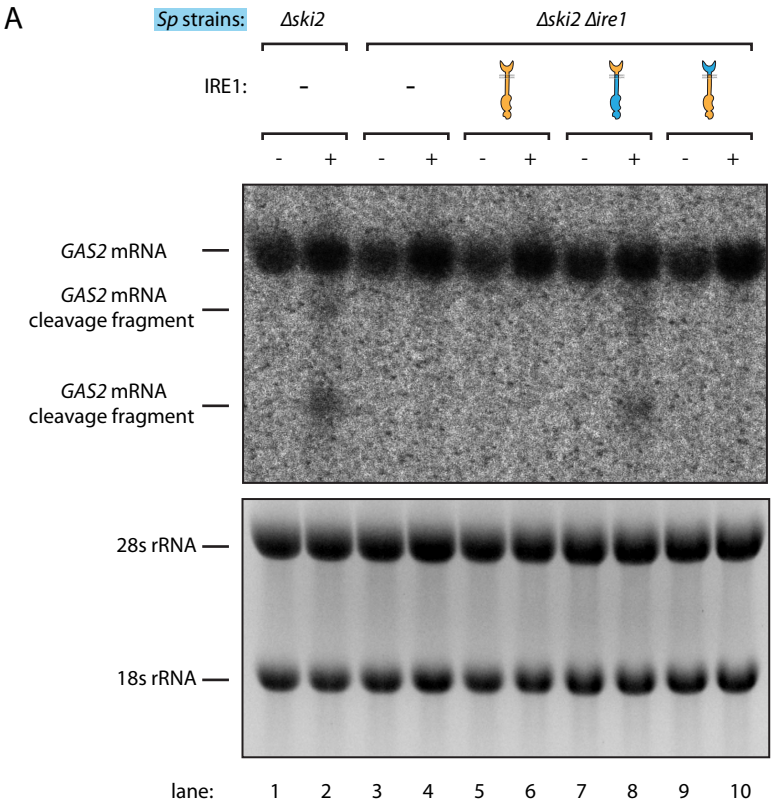

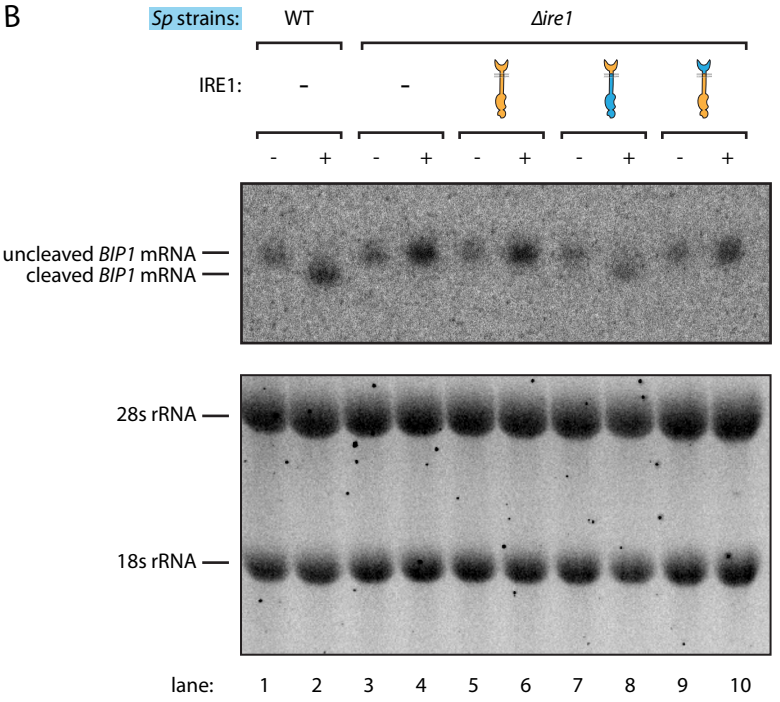

Fig. 1-figure supplement 2 Li et al.

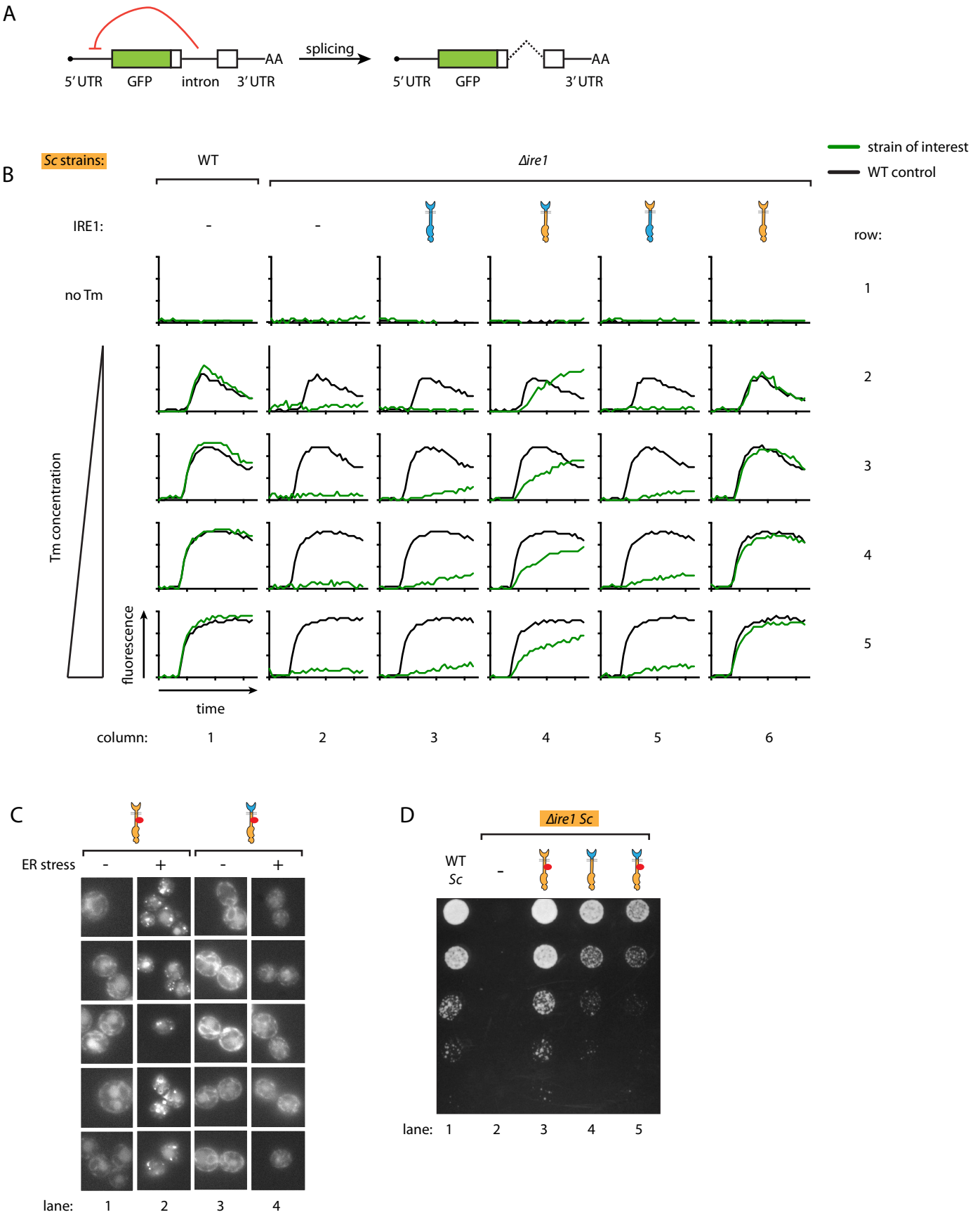

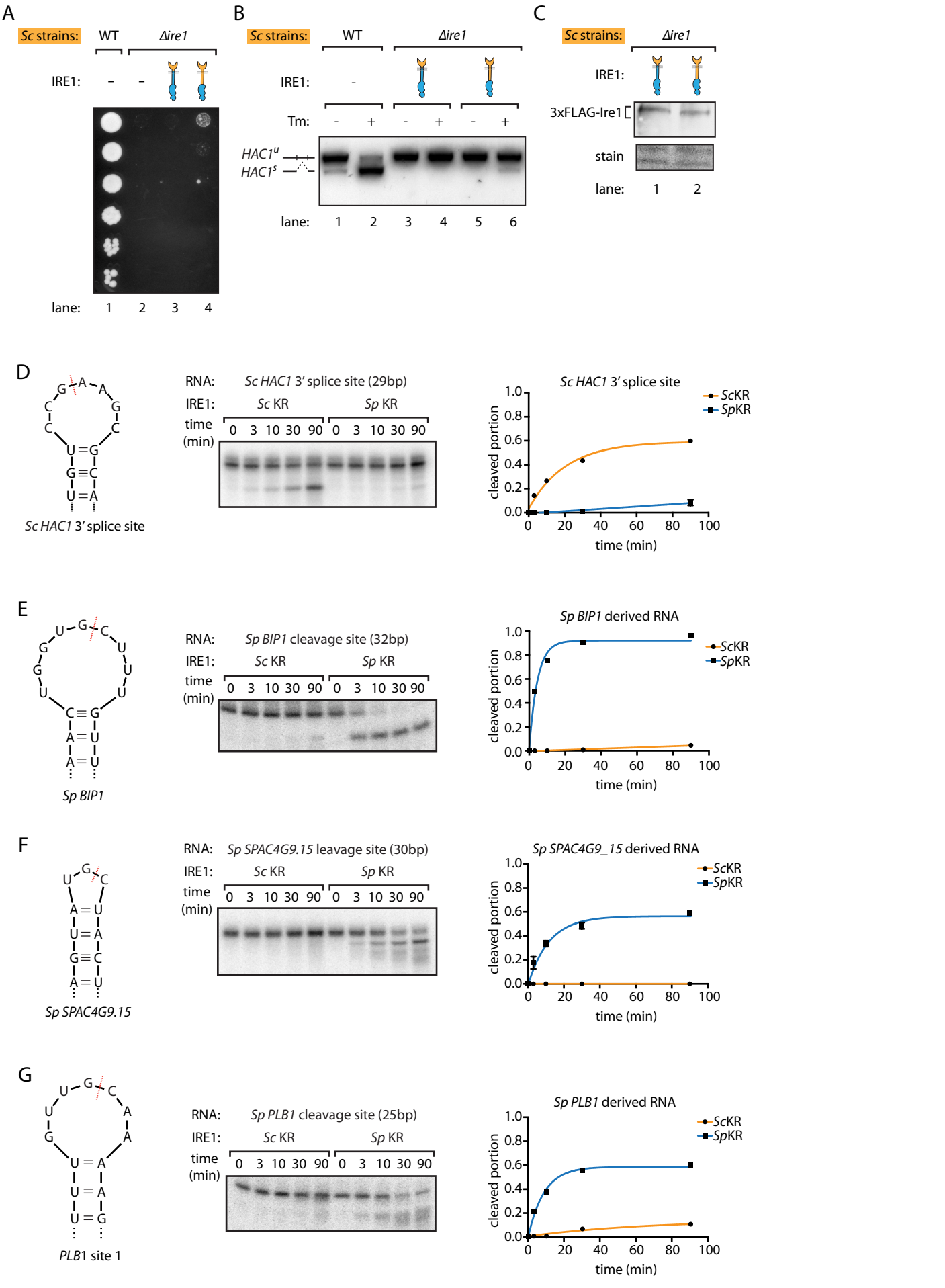
A
Sc strains:
WT
Δire1
IRE1:
lane: 1 2 3 4
B
Sc strains:
WT
Δire1
IRE1:
Tm:
HAC1u
HAC1s
lane: 1 2 3 4 5 6
C
Sc strains:
Δire1
IRE1:
3xFLAG-Ire1
stain
lane: 1 2
D
Sc HAC1 3′ splice site
RNA: Sc HAC1 3′ splice site (29bp)
IRE1: Sc KR Sp KR
time (min) 0 3 10 30 90 0 3 10 30 90
Sc HAC1 3′ splice site
ScKR
SpKR
cleaved portion
time (min)
E
Sp BIP1
RNA: Sp BIP1 cleavage site (32bp)
IRE1: Sc KR Sp KR
time (min) 0 3 10 30 90 0 3 10 30 90
Sp BIP1 derived RNA
ScKR
SpKR
cleaved portion
time (min)
F
Sp SPAC4G9.15
RNA: Sp SPAC4G9.15 leavage site (30bp)
IRE1: Sc KR Sp KR
time (min) 0 3 10 30 90 0 3 10 30 90
Sp SPAC4G9_15 derived RNA
ScKR
SpKR
cleaved portion
time (min)
G
PLB1 site 1
RNA: Sp PLB1 cleavage site (25bp)
IRE1: Sc KR Sp KR
time (min) 0 3 10 30 90 0 3 10 30 90
Sp PLB1 derived RNA
ScKR
SpKR
cleaved portion
time (min)

Fig 3 Li et al.

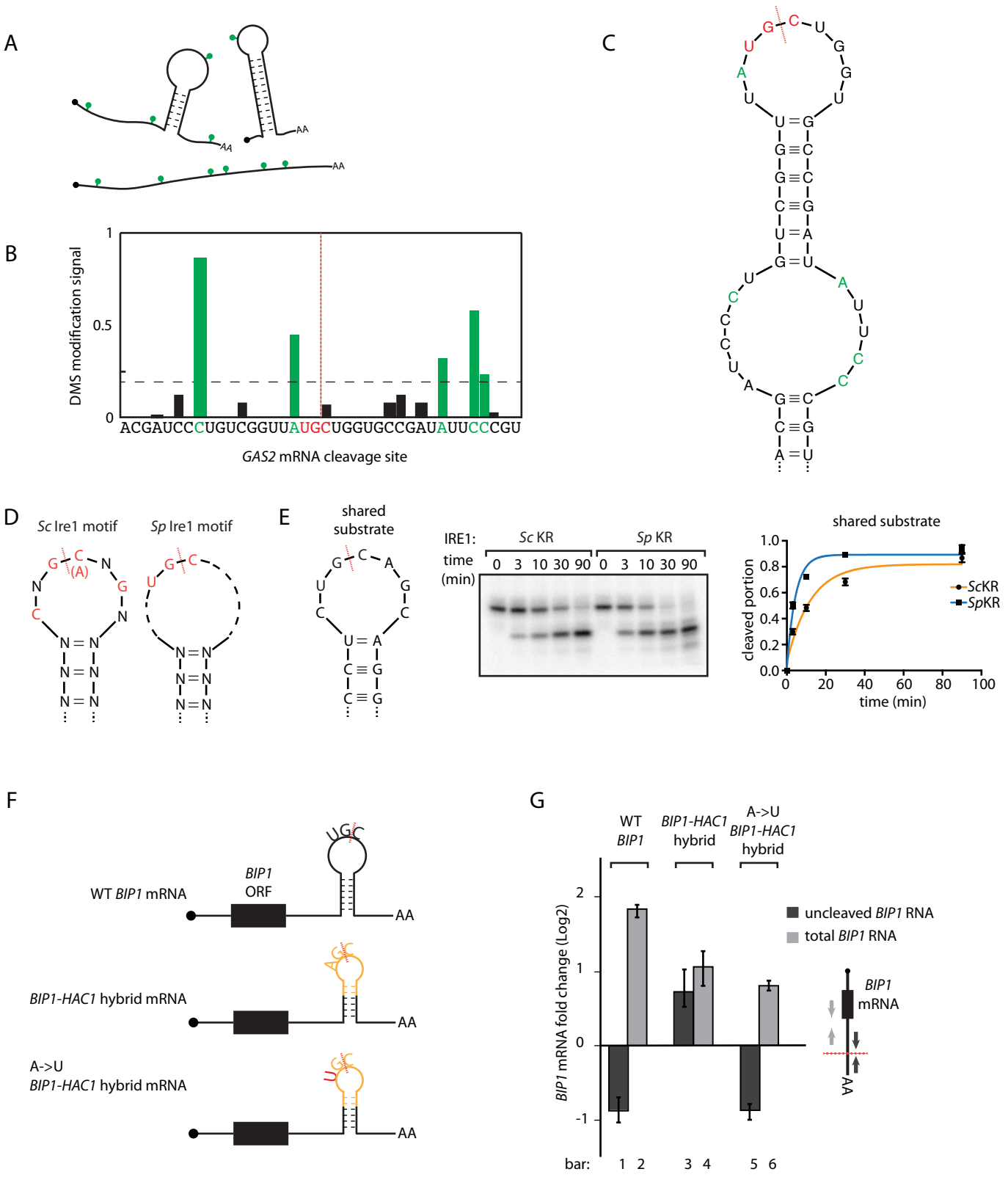
A
AA
AA
AA
B
DMS modification signal
1
0.5
0
ACGAUCCCUGUCGGUUAUGCUGGUGCCGAUAUUCCCGU
GAS2 mRNA cleavage site
C
D
Sc Ire1 motif
Sp Ire1 motif
E
shared substrate
IRE1:
Sc KR
Sp KR
time (min)
0 3 10 30 90 0 3 10 30 90
shared substrate
cleaved portion
time (min)
ScKR
SpKR
F
WT BIP1 mRNA
BIP1 ORF
AA
BIP1-HAC1 hybrid mRNA
AA
A->U
BIP1-HAC1 hybrid mRNA
AA
G
WT BIP1
BIP1-HAC1 hybrid
A->U BIP1-HAC1 hybrid
BIP1 mRNA fold change (Log2)
uncleaved BIP1 RNA
total BIP1 RNA
BIP1 mRNA
AA
bar: 1 2 3 4 5 6

Fig. 3-figure supplement 1 Li et al.

A

systematic ID	gene name	Ire1 cleavage site sequence
SPBC29A10.08	*GAS2*	ACGAUCCCUGUCGGUUAUGCUGGUGCCGAUAUUCCCGU
SPAC22A12.15c	*BIP1*	AACACCUAGUUAACUGGUGCUUUGUUAUCUUUGUAUUG
SPAC26A3.01	*SXA1*	AUUAUCGGUUUGUCAGUUGCCAUGACUAUUACUGGUAU
SPBC25H2.06c	*HRF1*	GAGCUAUUUGGCCUUCGUGCUAGUAAGGCUUGUGCUGU
SPAC1A6.04c	*PLB1*	UCCUUUGUGGCCUUUGUUGCAAAAGGGUCGUGAUGUCG
SPBP4G3.02	*PHO1*	AUUUGCAGUUAUGAAAUUGCCCUUCAAGACUAUAGCGA
SPCC970.03		CAUUUAUCGUUUCCGUCUGCCUCGCGCUAACGAUGUUC
SPBC29A10.08	*GAS2*	GCUGUCGCUUACGUUCGUGCUGCCGUUCGUGAUUCCAA
SPAC1A6.04c	*PLB1*	GUUGCCGAAAAGGCCAAUGCUGGCUUUAACACUCAGUCU
SPBP4G3.02	*PHO1*	AUCUUUGGAGGUGCCUAUGCUAAUAGCCUUGCAAAUUC
SPBC3D6.02	*BUT2*	CUUAGUGCUGACAUUCCUGCCAAGUCUAGCCGUCUCUU
SPAC56F8.07		CUUUUACUACGACAUGGUGCUGCAUGUUCGAGUUAUUU
SPCC830.08c	*YOP1*	GCCUUCUUUAGUAUCAAUGCUAUUGAAACUACUAACAA
SPAC4G9.15		GGAAUCGGUAAAGAGUAUGCUACUCAAUUAGCCAUGUC

B

9-membered loop

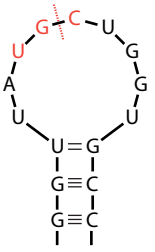

GAS2 site 1

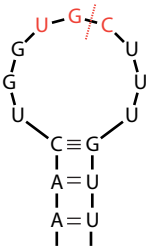

BIP1

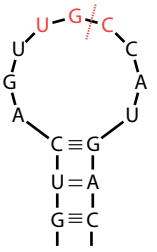

SXA1

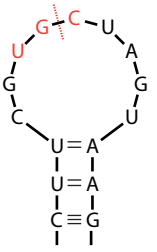

HRF1

7-membered loop

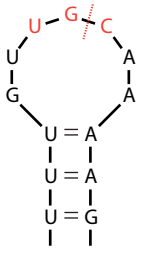

PLB1 site 1

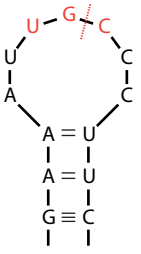

PHO1 site 1

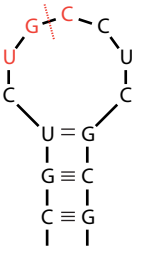

SPCC970.03

6-membered loop

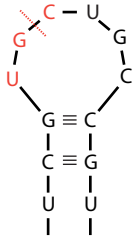

GAS2 site 2

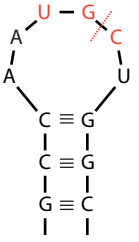

PLB1 site 2

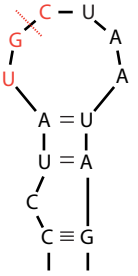

PHO1 site 2

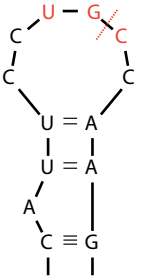

BUT2

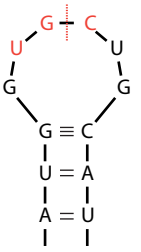

SPAC56F8.07

5-membered loop

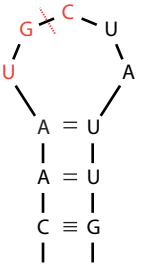

YOP1

3-membered loop

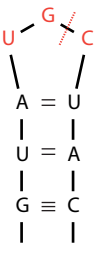

SPAC4G9.15

Fig 4 Li et al.

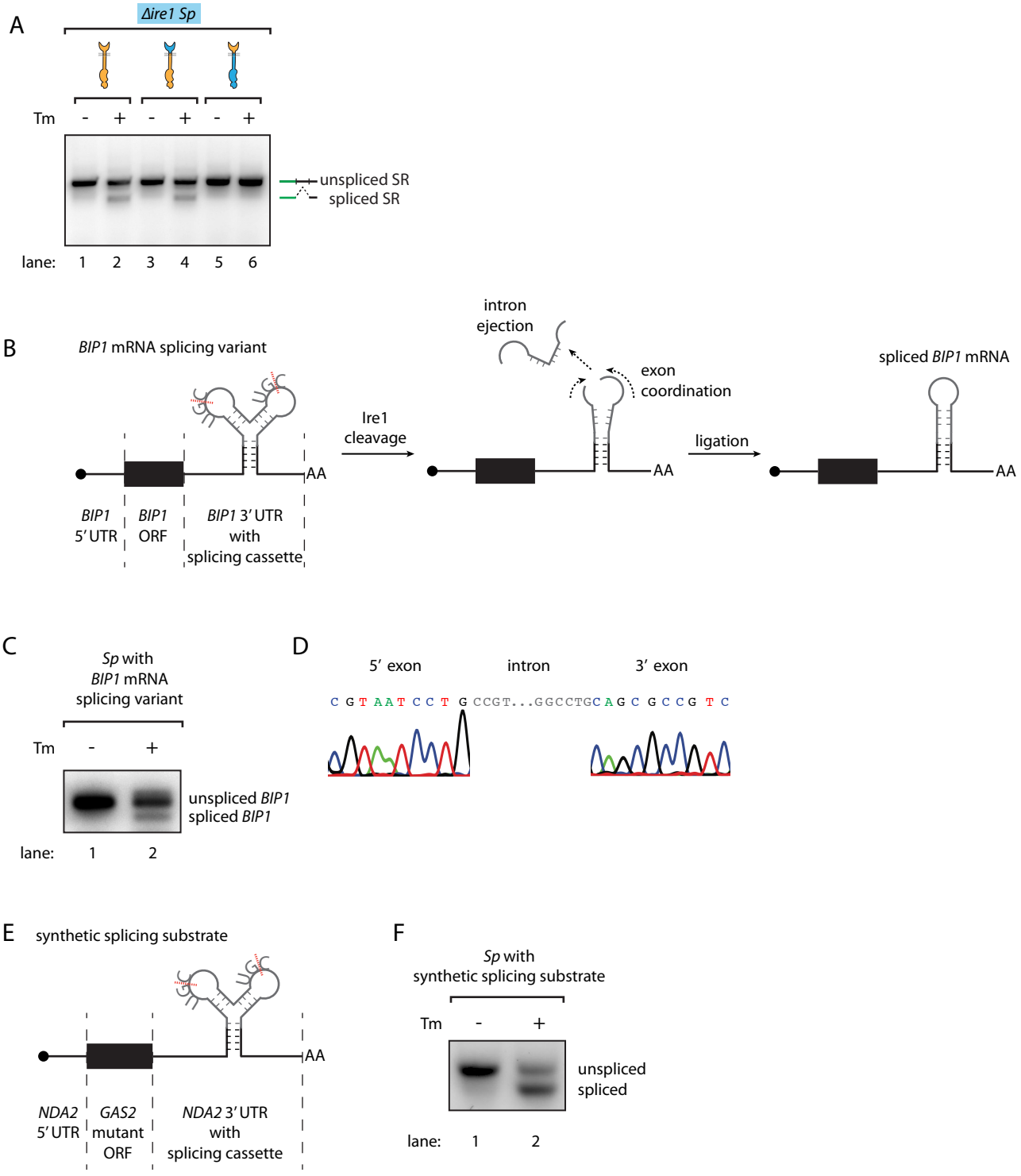
A
Δire1 Sp
Tm
- + - + - +
unspliced SR
spliced SR
lane: 1 2 3 4 5 6
B
BIP1 mRNA splicing variant
AA
BIP1 5′ UTR
BIP1 ORF
BIP1 3′ UTR with splicing cassette
Ire1 cleavage
intron ejection
exon coordination
ligation
spliced BIP1 mRNA
C
Sp with BIP1 mRNA splicing variant
Tm
- +
unspliced BIP1
spliced BIP1
lane: 1 2
D
5′ exon
intron
3′ exon
C G T A A T C C T G CCGT...GGCCTGCAGC G C C G T C
E
synthetic splicing substrate
NDA2 5′ UTR
GAS2 mutant ORF
NDA2 3′ UTR with splicing cassette
F
Sp with synthetic splicing substrate
unspliced
spliced

Fig. 4-figure supplement 1 Li et al.

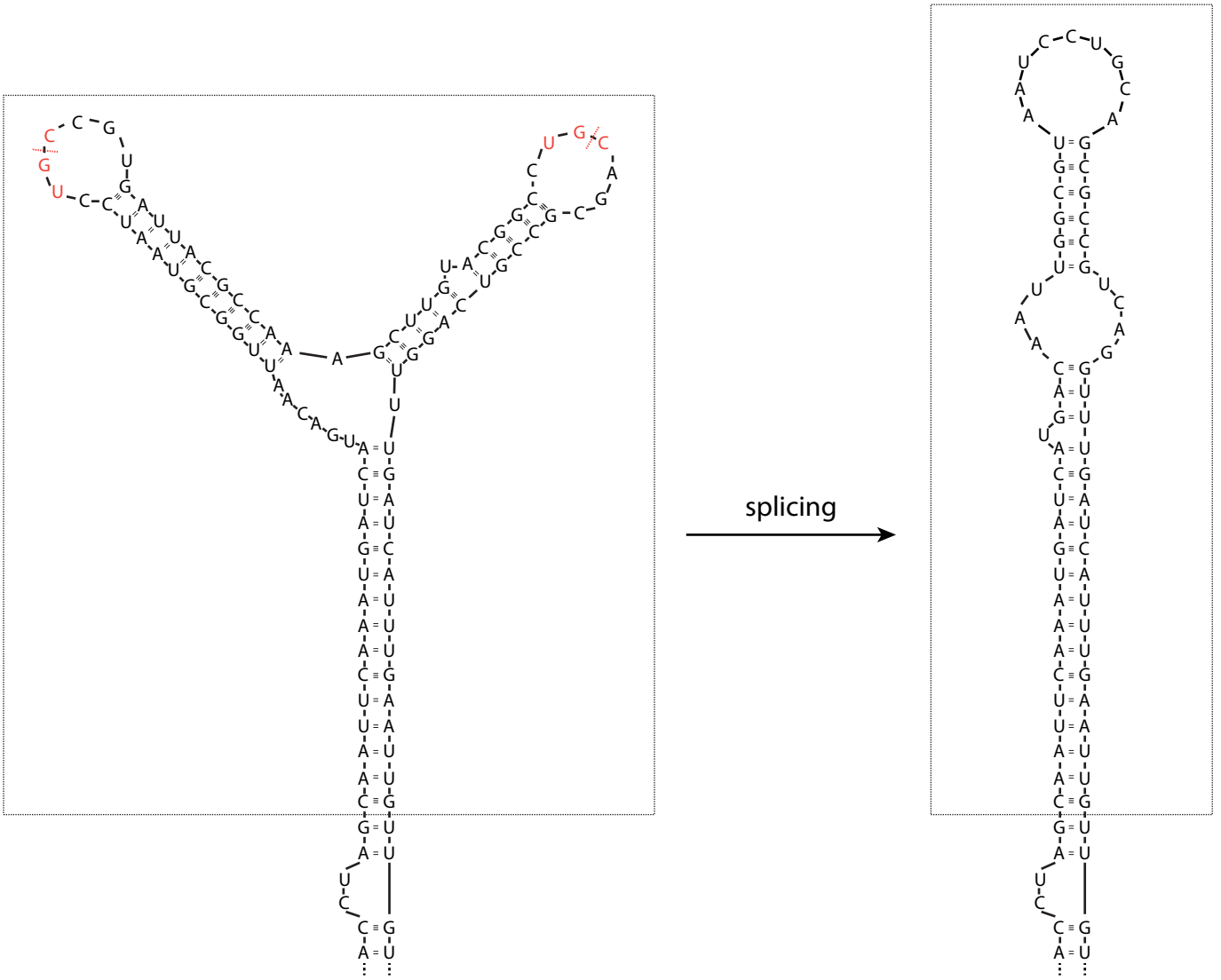

Fig. 4-figure supplement 2 Li et al.

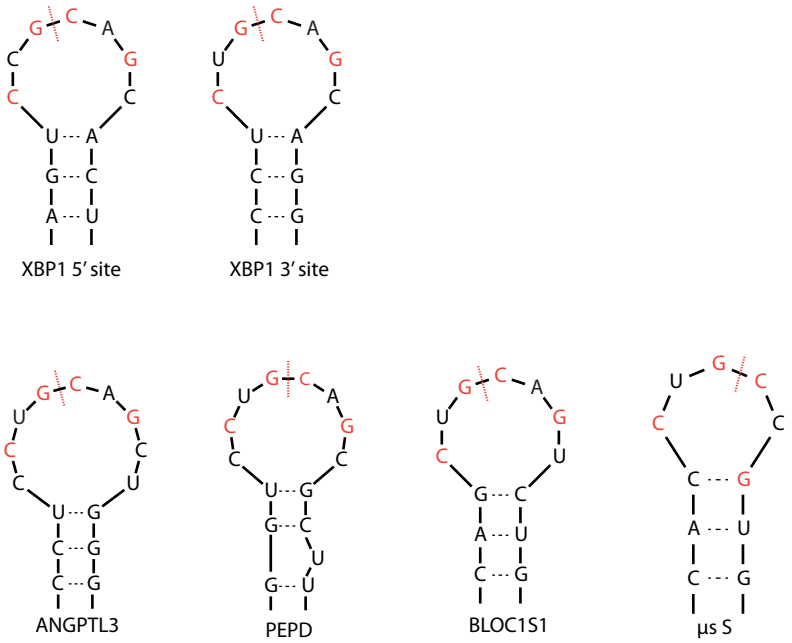

Fig. 4-figure supplement 3 Li et al.

A

```
IRE1alpha      1 LEKQLQFFQDVSDRIEKESLDGPIVKQLERGGRAVVKMDWRENITVPLQTDLRKFRTYKG
IRE1beta       1 RAKQLQFFQDVSDWLEKESEQEPLVRALEAGGCAVVRDNWHEHISMPLQTDLRKFRSYKG
Sc_IRE1        1 KSKKLEFLLKVSDRLEIENRDPPSALLMKFDAGSDFVIPSGDWTVKFDKTFMDNLERYRK
Sp_IRE1        1 YAKKLDFLIDVSDRFEVEERDPPSPLLQMLENNSKSVIGENWTTCLHSSLVDNLGKYRKY

IRE1alpha     61 GSVRDLLRAMRNKKHHYRELPAEVRETLGSLPDDFVCYFTSRFPHLLAHTYRAMELCSHE
IRE1beta      61 TSVRDLLRAVRNKKHHYRELPVEVRQALGQVPDGFVQYFTNRFPRLLLHTHRAMRSCASE
Sc_IRE1       61 YHSSKLMDLLRALRNKYHHFMDLPEDIAELMGPVPDGFYDYFTKRFPNLLIGVYMIVKEN
Sp_IRE1       61 DGSKILDILRVLRNKRHHYQDLPESVRRVLGDLPDGFTSYFVEKFPMLLLHCYHLVKDVL

IRE1alpha    121 RLFQPYYFHEPPEPQPPVTPDAL
IRE1beta     121 SLFLPYYPPDSEARRPCPGATGR
Sc_IRE1      121 LSDDQILREFLYS----------
Sp_IRE1      121 YEESQFKRYLEY----------
```

B